

Gold Nanoparticle-Incorporated Chitosan Nanogels as a Theranostic NanoplatforM for CT Imaging and Tumour Chemotherapy

Zhe Liu^{1-3,*}, Dong Zhou^{4,*}, Xuan Yan¹, Lan Xiao^{5,6}, Pei Wang¹⁻³, Junchao Wei¹⁻⁴, Lan Liao¹⁻³

¹The Affiliated Stomatological Hospital of Nanchang University, Nanchang, People's Republic of China; ²The Key Laboratory of Oral Biomedicine, Nanchang, People's Republic of China; ³Jiangxi Province Clinical Research Center for Oral Diseases, Nanchang, People's Republic of China; ⁴School of Chemistry and Chemical Engineering, Nanchang University, Nanchang, People's Republic of China; ⁵School of Mechanical, Medical & Process Engineering, Centre for Biomedical Technologies, Queensland University of Technology (QUT), Brisbane, Australia; ⁶Australia China Centre for Tissue Engineering and Regenerative Medicine, Kelvin Grove, Brisbane, Australia

*These authors contributed equally to this work

Correspondence: Junchao Wei; Lan Liao, Email weijunchao@ncu.edu.cn; Liaolan5106@ncu.edu.cn

Purpose: The translation of nanocarrier-based theranostics into cancer treatment is limited by their poor cellular uptake, low drug-loading capacity, uncontrolled drug release, and insufficient imaging ability.

Methods: In this study, novel hybrid nanogels were fabricated as theranostic nanocarriers by modifying chitosan (CTS)/tripolyphosphate (TPP) nanoparticles (NPs) with polyacrylic acid (PAA) and further conjugating cysteine-functionalized gold nanoparticles (AuNPs).

Results: The resultant nanogels, referred to as CTS/TPP/PAA@AuNPs (CTPA), exhibited excellent colloidal stability and a high encapsulation rate of 87% for the cationic drug doxorubicin (DOX). In the tumour microenvironment, the acidic pH and over-expression of lysozyme triggered CTPA@DOX to degrade and emit smaller nanoblocks (30–40 nm), which sequentially released the drug in a tumour-responsive manner. Cellular uptake experiments demonstrated that CTPA facilitates the entry of DOX into the cytoplasm. Furthermore, as visualised through AuNP-mediated computed tomography (CT) imaging, CTPA@DOX enabled favourable accumulation in the tumour. Our in vitro and in vivo data demonstrated that CTPA enabled advanced tumour cell-targeting delivery of DOX, which showed greater anti-tumour activity and biosafety than free DOX.

Conclusion: The natural polymer CTS was developed for degradable nanogels, which can precisely track drugs with high antitumour activity. Additionally, the surface adjustment strategy can be assembled to achieve cationic drug loading and high drug-loading capacity, controlled drug release, and sufficient imaging ability. Therefore, multifunctional CTPA enables efficient drug delivery and CT imaging, which is expected to provide a valuable strategy for designing advanced theranostic systems.

Keywords: theranostic nanomaterial, degradability, computed tomography imaging, hybrid nanogel

Introduction

Theranostic nanocarriers have attracted increasing attention for cancer treatment.^{1,2} As multifunctional devices, theranostic nanocarriers can be effectively combined with tumour markers to detect various diseases at low concentrations with high sensitivity.³ Additionally, theranostic nanocarriers can reduce drug toxicity and meet low-dosage drug requirements.⁴ Theranostic nanocarriers deliver drugs to the action site passively and/or actively, and also concurrently provide valuable diagnostic information, such as tumour location, drug distribution, and tumour response to treatment.^{5,6} Currently, there are several types of theranostic nanocarriers, including magnetic nanoparticles (NPs), carbon quantum dots, and gold nanoparticles (AuNPs). Magnetic NPs can control the accumulation of drugs in specific parts of the tumour and reduce the general distribution of drugs, whereas carbon quantum dots can be prepared as electrochemical sensors by utilising their large surface area. AuNPs can be used as electrochemical sensors owing to their strong surface

properties and easy modification.^{7,8} Ideally, theranostic nanocarriers should enable a combined effective drug delivery and imaging diagnosis, which is a significant challenge for nanotechnology.⁹ To achieve effective tumour-targeted drug delivery, carriers should enable stability in long-term circulation, proper drug distribution, deep tumour penetration, controlled drug release, and enhanced cellular uptake.^{10,11} Generally, these functions largely depend on the properties of the particles, including size, charge, degradability, elasticity, and surface chemistry, which need to be elegantly tailored.^{12,13} Furthermore, theranostic nanocarriers should enable the efficient conjugation of therapeutics and diagnostics, thereby satisfying the dosing demands of imaging and therapeutic approaches.¹⁴

Recently, nanogels with diverse physicochemical properties have received extensive attention.^{15,16} They offer unique advantages for drug delivery. For instance, the swelling and degradation properties of nanogels can be leveraged to design intelligent carriers for tumour-targeted drug release.^{17,18} Furthermore, the softness of nanogels minimises their uptake by the reticuloendothelial system (RES), facilitating a long circulation time.^{19,20} In addition, deformability-integrated enzyme-degradability imparts nanogels with the desired capability of deep tumour penetration, which is beneficial for treating solid tumours.^{21,22} Recently, there has been increasing interest in the development of polysaccharide-based nanogels,²³ predominantly chitosan (CTS)^{24,25} and hyaluronic acid nanogels.²⁶ Among these, CTS nanogels possess excellent biosafety and abundant reactive groups on their molecular backbone.²⁷ Such groups provide CTS nanogels with a wide availability of conjugating multiple cargos, and also endow CTS nanogels with favourable bioactivity. Considering the superiority of theranostics in personalised drug delivery, it is feasible to reinforce CTS nanogel-based carriers with the capability of imaging diagnosis in a coordinated manner, thus enabling precise therapy against tumours.

AuNPs have great potential in theranostics owing to their excellent imaging ability. The unique surface plasmon resonance property and X-ray attenuation ability of AuNPs render them appropriate for fluorescence imaging, magnetic resonance imaging (MRI), and computerized tomography (CT) imaging.^{28–30} Additionally, their high affinity to thiols enables AuNPs to carry various drugs, including genes and chemotherapeutics.^{31,32} However, drug payloads limit their further application. To address this issue, incorporation of AuNPs with other larger organic structures, such as nanogels, liposomes, and dendrimers, to form nanocomposites is expected to be an effective approach.^{33–35} Under these circumstances, AuNPs are responsible for imaging, whereas organic components with a high surface area are used to carry therapeutics.

In the current study, to develop a theranostic nanocarrier with favourable physicochemical properties and enhanced versatility, this nanocarrier combines high-efficiency antitumour activity and imaging capability (Figure 1). During preparation, hydrophilic polyacrylic acid (PAA) with a low molecular weight was applied to enhance the colloidal stability of CTS NPs through surface-coating modification. Additionally, the introduction of PAA supported the loading of AuNPs and improved the entrapment rate of the cationic drug doxorubicin (DOX). Specifically, functionalized AuNPs were grafted onto the surface of the modified nanogels through an amidation reaction, and DOX was adsorbed into the interior of the nanogels through electrostatic interactions, ultimately resulting in CTS/tripolyphosphate (TPP)/PAA@AuNPs (CTPA)@DOX. Upon reaching the tumour, the accumulation of CTPA@DOX was visualised through AuNP-mediated CT imaging. Furthermore, CTPA@DOX tended to degrade and release drugs in response to the tumour microenvironment (in enzyme- and acid-triggered manners), which resulted in high-performance antitumour therapy. The results showed that the carrier was expected to possess high conjugation efficiency for therapeutic and diagnostic agents, greater drug delivery and imaging capacities, and outstanding biosafety.

Materials and Methods

Materials

CTS, chloroauric acid ($\text{HAuCl}_4 \cdot 4\text{H}_2\text{O}$), TPP, PAA (MW:2000 Da), sodium borohydride (NaBH_4), 1-(3-(dimethylamino)propyl)-3-ethylcarbodiimide hydrochloride (EDC·HCl), and N-hydroxysuccinimide (NHS) were purchased from Sinopharm Chemical Reagent Co., Ltd. (Shanghai, China). Unless otherwise stated, all chemical reagents were of analytical grade. Dulbecco's modified Eagle's medium (DMEM) and foetal bovine serum (FBS) were obtained from GIBCO Co., Ltd. (California, USA). Other biological materials were procured from Sigma-Aldrich (MO, USA). The

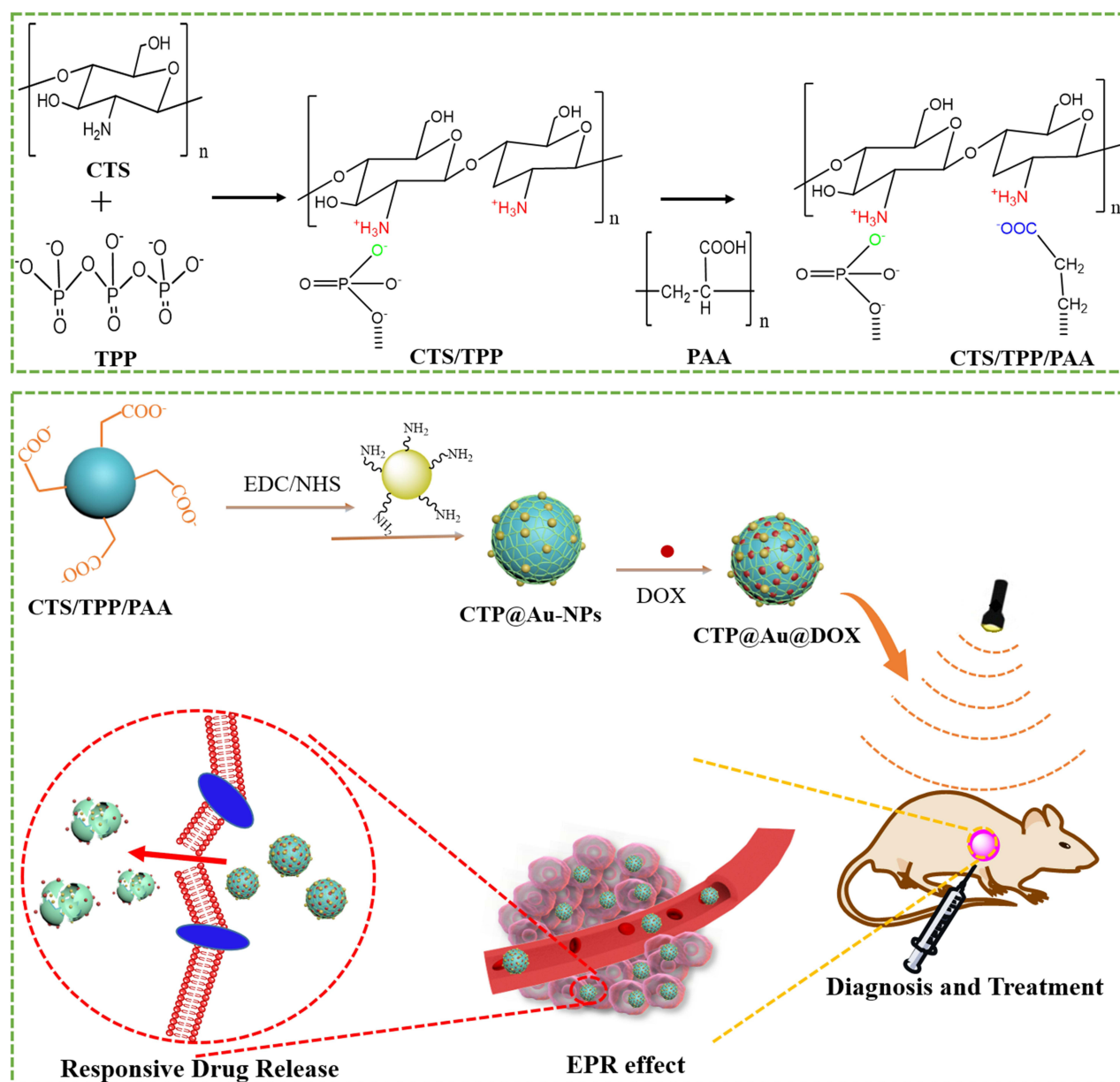


Figure 1 Schematic synthesis of CTS/TPP/PAA@AuNPs (CTPA) and schematic illustration of CTPA theranostics, which simultaneously acts as a drug carrier for chemotherapy and a contrast agent for CT diagnosis.

CAL-27 cells were purchased from the Cell Bank of the Type Culture Collection of the Chinese Academy of Sciences (Shanghai, China). The acridine orange/ethidium bromide (AO/EB) double fluorescence staining kit was purchased from Shanghai Beibo Biotechnology Co. Ltd. The terminal deoxynucleotidyl transferase-mediated dUTP-biotin nick end labelling (TUNEL) apoptosis detection kit (colour method) was purchased from Biyuntian Biotechnology Co. Ltd.

Preparation of CTPA Nanogels

Briefly, a 1 mg/mL CTS solution (pH 5.5) was prepared by dissolving CTS in an acetic acid solution (1%). TPP aqueous solution (0.1 mg/mL) was added dropwise to the stirred CTS solution at 6 s intervals, resulting in the formation of CTS NPs (CTS/TPP). Next, the CTS/TPP solution was added to an aqueous PAA solution (10 mg/mL) and stirred for 10 min. Finally, the mixture was dialysed in a dialysis bag (MWCO:8000–14000 Da) to obtain the CTS/TPP/PAA (CTP) nanogels.

AuNPs were prepared using the NaBH₄ reduction method. Briefly, HAuCl₄ (2.5 mL) dissolved in ultrapure water (25 mL) was added dropwise to the NaBH₄ solution (5 mg/mL, 2 mL) and stirred for 20 min. Subsequently, 1 mL of cysteine solution (17 mM) was added to the above mixture. After reacting overnight, the as-prepared cysteine-functionalized AuNPs were purified using the dialysis method described above.

AuNP-loaded CTS nanogels were then prepared. Briefly, 1 mL of EDC·HCl (5 mg/mL)/NHS (5 mg/mL) was added to 30 mL of CTP nanogel solution for 2 h to activate the carboxyl groups. Cysteine-functionalized AuNPs were added to the above reaction solution in accordance with a volume ratio of 1:1 and stirred at 25 °C for 2 h. After centrifugation (10,000 rpm, 10 min) and purification (dialysis, MWCO: 8000–14000 Da), the resulting nanogel (CTPA) was obtained. The content of AuNPs in the CTPA was detected using an inductively coupled plasma optical emission spectrometer (ICP-OES; Prodigy, USA).

Characterization

Scanning electron microscopy (SEM; ZEISS Sigma 300, Germany) was used to characterise the morphology and size of the CTPA. The hydrodynamic diameter and zeta potential of the different formulations were tested using dynamic light scattering (DLS; Nano ZS 90, Malvern). The UV absorbance spectra of the different samples were recorded using a ultraviolet-visible (UV-vis) spectrophotometer (UV-5200, China).

Loading and Release of DOX

Initially, 5 mL of CTPA aqueous solution was mixed with 1 mL of DOX aqueous solution (2 mg/mL) and stirred for 12 h. The mixture was then placed in a dialysis bag (MW: 8000–14000 Da) for dialysis against phosphate-buffered saline (PBS). The dialysate was collected to measure the UV absorbance at 490 nm.

To test the degradation ability, CTPA@DOX was submerged in a PBS solution (pH 5.0) containing lysozyme at a concentration of 5.0 µg/mL. After incubation for 24 h, the samples were analysed using transmission electron microscopy (TEM; JEM-210003040700, Japan).

To evaluate DOX release, 1 mL of CTPA@DOX dialysis samples was first immersed in PBS solutions with different pH values (5.0, 6.5, and 7.4). At defined time points, 3 mL aliquots were removed to measure the amount of released DOX using UV-vis spectrum analysis, followed by the addition of fresh PBS to maintain volume consistency. To assess the enzyme-sensitive property, CTPA@DOX was incubated in PBS containing 0, 5, and 10 µg/mL of lysozyme, and the released amounts of DOX at predetermined time points were detected using the method described above.

X-Ray Attenuation Measurements

Several CTPA@DOX samples with different concentrations of AuNPs (7.0, 4.0, 2.0, 0.5, and 0.25 mg/mL) were prepared. The CTPA@DOX samples were then suspended in a 96-well plate containing agar. A well without any samples was used as the control. Subsequently, the plate was subjected to X-ray attenuation measurements using a CT system (SkyScan 1176, Germany).

In vitro Cytotoxicity and Cell Uptake

The cytotoxicities of CTPA and CTPA@DOX were assessed using the Cell Counting Kit-8 (CCK-8) assay. Briefly, the human tongue squamous cell carcinoma (OSCC) cell line, CAL27, was incubated into culture flasks. Upon reaching 80% confluence, the cells were digested and seeded into 96-well plates (1×10⁵ cells/well) for 24 h. The culture medium in each well was then replaced with 100 µL of fresh DMEM containing DOX, CTPA@DOX, and empty CTPA. The DOX and CTPA@DOX groups had equivalent DOX concentrations (0.75, 1.5, 2, 3, and 6 µM), and the amount of empty CTPA was identical to that used to prepare CTPA@DOX. After 24 h of incubation, the cells were washed twice with PBS, and 100 µL of DMEM containing 10 µL of CCK-8 solution was added to each well. Finally, optical density was measured at 450 nm using a microplate reader (Tecan 200 Pro, Switzerland).

AO/EB double fluorescence staining was used to assess the anti-tumour effects in vitro. Briefly, CAL27 cells were seeded onto cover slips in a 12-well plate (2×10⁵ cells/well). After incubation for 48 h, the initial medium was replaced with fresh medium containing DOX and CTPA@DOX at an identical DOX concentration (2 µM), and the cells were

treated for 24 h. Then, the coverslips were washed with PBS and stained with AO/EB solution. Finally, confocal fluorescence microscopy (CLSM, Nikon A1SiR, Japan) was used to observe the live/dead cells.

Cellular uptake of CTPA@DOX by CAL27 cells was evaluated using CLSM. First, CAL27 cells at a density of 1×10^5 cells/dish were seeded into 20 mm confocal cell culture dishes for 24 h. Then, DOX and CTPA@DOX at the same DOX concentration (2 μ M) were added to treat the cells. Subsequently, the medium was discarded at pre-designed points (4 and 24 h). After washing three times with PBS, the cells were fixed with 4% paraformaldehyde for 30 min. The cells were then washed several times and incubated with 4,6-diamino-2-phenylindole (DAPI) in the dark for 5 min. Finally, after washing three times, the cells were observed using CLSM.

CAL27 cells were seeded in 6-well plates at a density of 5×10^4 cells/well for 24 h. After that, DOX and CTPA@DOX at a same DOX concentration (2 μ M) were added to treat the cells and the cells were further incubated for another 4 h and 24 h. After washed 3 times with PBS, they were then digested with trypsin and collected in centrifuge tubes. Finally, untreated cells were used as a control, and the suspended cells were filtrated and detected by flow cytometry (Cytotoflex 0314, Beckman, USA).

In vivo CT-Imaging and Anti-Tumour Ability Evaluation

All animal procedures were approved by the Animal Care and Use Committee of Nanchang University and conformed to the National Institutes of Health Guide for the Care and Use of Laboratory Animals. Experimental mice were obtained from Charles River Experimental Animal Co. Ltd. (Beijing, China). Subcutaneous OSCC models were established by injecting 1×10^7 CAL27 cells into the right oxter of mice. Mice bearing a tumour of 150 mm³ in size were subjected to the following experiments.

Micro-CT scans were performed to detect the regions of interest before and 60 min after the injection of 1 mL of CTPA@DOX through the tail vein. Scanning voltage and current were 100 kV and 80 mA, respectively.

To evaluate the anti-tumour efficacy and biosafety of CTPA@DOX in vivo, mice were separated into three groups (n=6). Firstly, 1 mL of different solutions (PBS, DOX, CTPA@DOX, DOX dose: 4 mg/kg) was injected into mice via a one-time intravenously injection. And then, the antitumor activity of different drugs on tumor mice was observed for 21 days. Tumour volume and body weight were recorded every 2 d. On day 21 post-injection, the main organs (heart, liver, spleen, lungs, and kidneys) and tumours were harvested for histological analysis, including haematoxylin and eosin (H&E) staining and TUNEL assays. Simultaneously, blood samples were collected for biochemical examinations.

Results and Discussion

Preparation of Hybrid Nanogels

Nanogels are suitable for standard drug delivery. To further improve their versatility, hybrid CTS nanogels with enhanced colloidal stability and imaging capability have been developed as a theranostic strategy. Briefly, CTS was mixed with oppositely charged TPP to form ionically crosslinked CTS NPs (CTS/TPP) with a hydrodynamic size of 158.2 ± 2.3 nm (Table 1). Subsequently, CTS/TPP was added to a solution of the oligomer PAA to form colloiddally stable and negatively charged nanocarriers (CTS/TPP/PAA; CTP). CTP efficiently incorporated cysteine-functionalized AuNPs (4–5 nm) (Table 1) through amidation reactions, ultimately generating a core-satellite structure (Figure 2A and B). The as-prepared

Table 1 Hydrodynamic Size, Zeta Potential, and Drug-Loading Capacity of Different Formulations

Sample	Size (nm)	Zeta (mV)	EE (%) ^a
AuNPs	4±2	-12.1±1.5	–
CTS/TPP	158.2±2.3	31±4.7	–
CTPA	172.3±2.1	-28.1±3.8	–
CTPA@DOX	198.7±3.2	-27.4±3.1	87.1±4.6

Note: ^aEncapsulation efficiency (EE) = $100 \times W_e/W_0$, where W_0 is the total drug for loading and W_e is the entrapped drug.

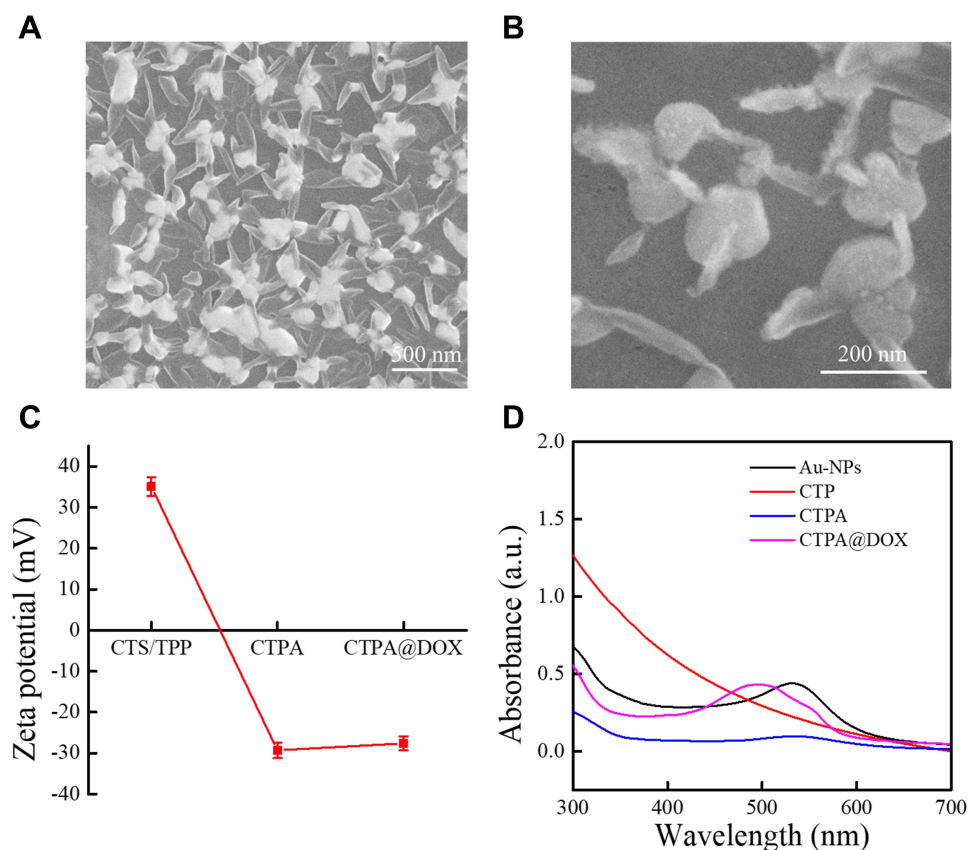


Figure 2 SEM images of CTPA (**A** and **B**); (**C**) Zeta-potential changes after CTS/TPP transformed to CTPA and then loading with DOX; (**D**) UV-vis absorbance spectrum of AuNPs, CTP, CTPA, and CTPA@DOX.

nanogels, CTS/TPP/PAA@AuNPs (CTPA), had a hydrodynamic size of 172.3 ± 2.1 nm (Table 1), or 153.1 ± 5.6 nm, as determined using SEM. This slight difference in size measurements is due to the formation of a hydrated layer on the exterior surface of the nanogels. Furthermore, CTS, as a cationic molecule, imparted a positive surface charge on CTS/TPP. The negatively charged PAA covered CTS/TPP to adjust the surface potential from 31 ± 4.7 to -28.1 ± 3.8 mV (Table 1). This charge conversion led to a high encapsulation rate of $87.1 \pm 4.6\%$ for cationic drug DOX (Figure 2C). The resultant drug-loaded nanoplatform (CTPA@DOX) exhibited a negatively charged potential of -27.4 ± 3.1 mV with a hydrodynamic size of 198.7 ± 3.2 nm (Table 1), which was advantageous for long circulation.^{36,37} Therefore, CTPA@DOX has great potential for ensuring an effective cargo delivery.

UV-vis spectroscopy measurements were used to demonstrate the successful fabrication of CTPA@DOX. The peak located at 530 nm is a typical absorption peak of AuNPs, which is present in the CTPA spectrum (Figure 2D). This result shows that AuNPs were successfully conjugated to the nanogels. Because the connection of AuNPs was mediated by cysteine and PAA, it also demonstrated that complex nanogels comprising CTS, TPP, and PAA were successfully constructed. Furthermore, in the spectrum of CTPA@DOX, a clear characteristic peak appeared at 490 nm, which was ascribed to DOX (Figure 2D), suggesting that CTPA can entrap DOX.

Degradation and Drug Release Assays in vitro

Lysozyme is highly synthesised in human carcinomas, generating a high concentration in lesions.³⁸ To assess lysozyme degradability, CTPA@DOX was incubated in a weakly acidic condition containing $5 \mu\text{g/mL}$ lysozyme. TEM images showed that CTPA@DOX decomposed and released smaller nano blocks of 30–40 nm (Figure 3A and B). Such biodegradability provides many advantages. As indicated, it can endow nanocarriers with size-variable capability, which is a key element dominating intratumour distribution.^{39,40} In general, NPs with a relatively large size (100–200 nm) enable prolonged circulation. Upon reaching tumour sites, shrinkable particles are likely to achieve high tumour-

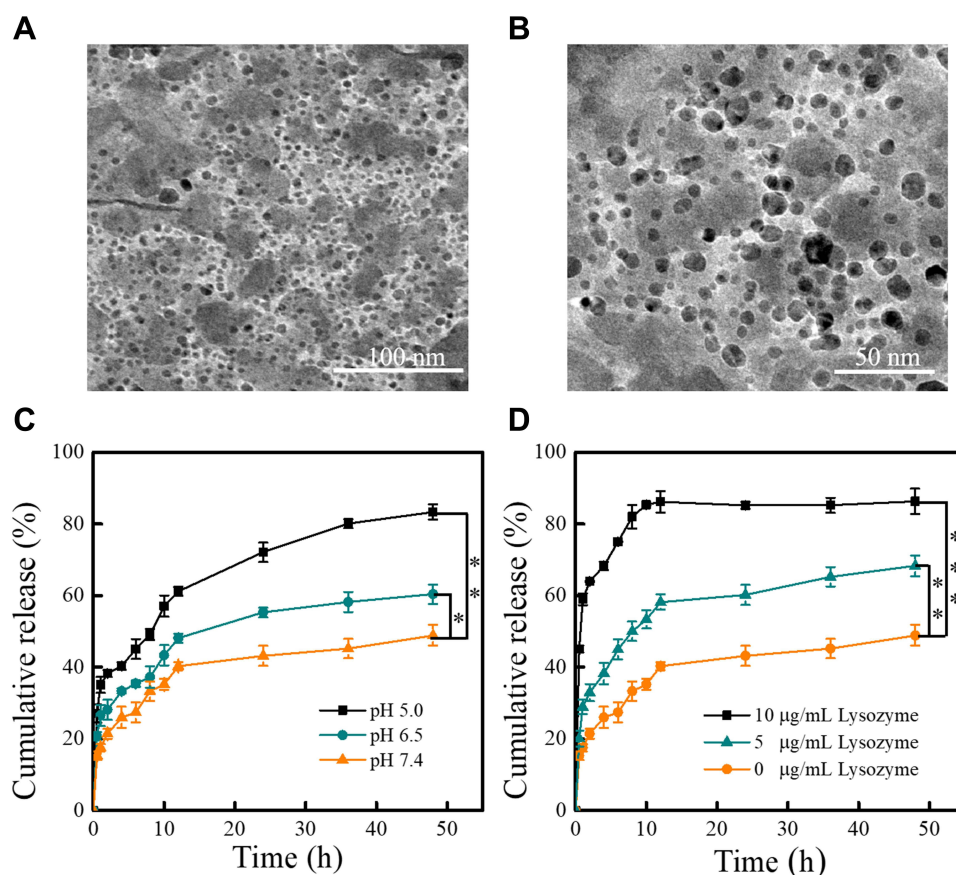


Figure 3 TEM images of CTPA@DOX incubated in weakly acidic PBS solution (pH 5.0) containing 5 µg/mL lysozyme for 24 h (**A** and **B**); (**C**) Drug release curves of CTPA@DOX in PBS solution with different pH values (7.4, 6.5, and 5.0); (**D**) Drug release curves of CTPA@DOX with different concentrations of lysozyme (0, 5.0, and 10.0 µg/mL). * indicates $P < 0.05$, ** indicates $P < 0.01$, and *** indicates $P < 0.001$.

penetrating efficiency and favourable tumour distribution. Another merit of these nanocarriers is that they allow rapid renal elimination of degradation products, leading to concerns over permanent toxicity.⁴¹ Therefore, CTPA@DOX can be used as a reliable tool for tumour eradication and biosafety.

Nanogels represent a class of carriers that allow smart drug delivery to specifically target tumour cells. To confirm the drug release in a tumour-specific manner, CTPA@DOX was first placed into PBS solutions with different pH values to simulate various microenvironments, namely pH 7.4 (physiological blood circulation), pH 6.5 (tumour stroma), and pH 5.0 (endo/lysosomes).⁴² Increasing the pH accelerated drug release and elevated the cumulative drug release rate (Figure 3C). This pH-dependent sensitivity was profoundly related to the fact that the protonation of amino groups in CTS molecules caused a swollen state of the nanogels through the repulsive force of $-\text{NH}_3^+$.⁴³ This feature improves drug bioavailability and prevents drug release before reaching the target (tumour). In particular, when exposed to an acidic environment (pH 5.0), DOX maintained sustained release for up to 48 h, which guaranteed a long-term anticancer effect (Figure 3C). The drug release behaviour of CTPA@DOX was examined in the presence of lysozyme. As shown in Figure 4D, the release rate and cumulative release rate of DOX were significantly enhanced in the lysozyme solution. When treated with 10 µg/mL lysozyme, nearly 80% of the DOX was released within the first 10 h (Figure 3D). This unique release profile resulted from the degradation of the nanogels. Based on these results, the acid- and lysozyme-sensitivity renders CTPA@DOX a useful drug carrier targeting tumours, maximising the therapeutic efficiency and minimising the side effects.

Evaluation of Cytotoxicity in vitro

The biocompatibility of CTPA and toxicity of CTPA@DOX to CAL27 cells were assessed using the CCK-8 assay. Empty CTPA did not affect the viability of CAL27 cells, even at high concentrations (Figure 4A). This suggested good

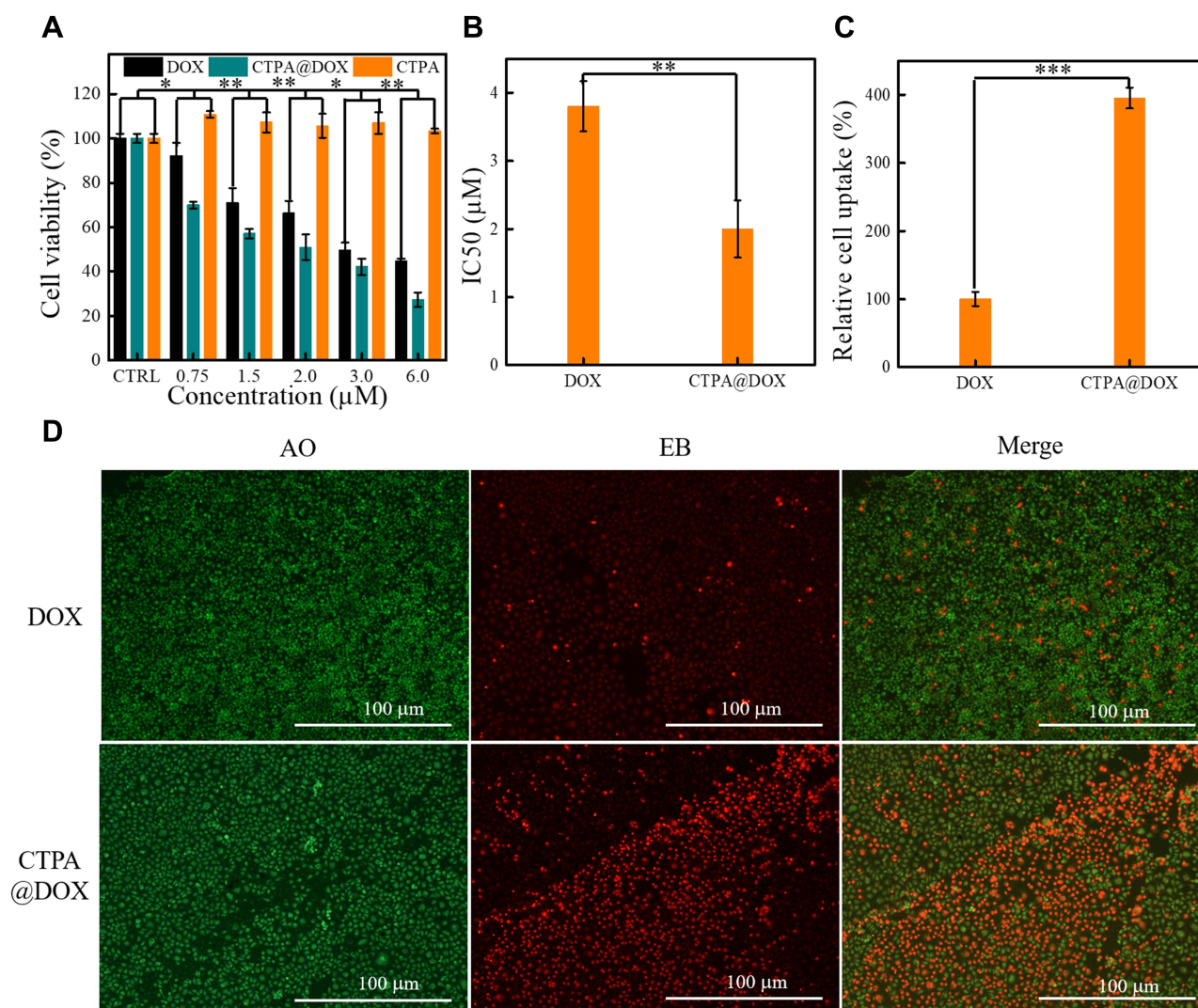


Figure 4 Evaluation of biocompatibility and toxicity. **(A)** Relative viability of CAL27 cells after treatment with DOX, CTPA@DOX, and CTPA; **(B)** IC₅₀ values of DOX- and CTPA@DOX-treated CAL27 cells after 24 h; **(C)** The quantitative red fluorescence intensity of CAL27 cells after treatment with DOX and CTPA@DOX for 24 h in AO/EB assays; **(D)** AO/EB staining images of CAL27 cells treated with DOX and CTPA@DOX. *Indicates $P < 0.05$, **Indicates $P < 0.01$, and ***Indicates $P < 0.001$.

biocompatibility of CTPA and maintained excellent colloidal stability under neutral conditions, thus avoiding negative effects on cell growth. Increasing the amount of DOX led to a decrease in the cell viability. A similar trend was observed in the CTPA@DOX group. However, the viability of CTPA@DOX was notably lower than that of free DOX at all the concentrations. The IC₅₀ value of free DOX (3.7 μM) at 24 h was nearly 2-fold higher than that of CTPA@DOX (1.9 μM) (Figure 4B), indicating CTPA@DOX that was more effective in killing CAL27 cells than free DOX, suggesting this nanogel formulation increased the half-life of the drug and showed continuous release to achieve sustained and efficient anti-tumor effect. AO/EB staining assays were performed to confirm the cytotoxicity of free DOX and CTPA@DOX. The proportion of dead cells emitting red fluorescence varied significantly, and more cells died after treatment with CTPA@DOX (Figure 4D). Quantitative analysis of red fluorescence also showed that cell death in the CTPA@DOX group was 3.9-fold higher than that in the free DOX group (Figure 4C). Collectively, CTPA@DOX exhibited higher anti-tumour activity than free DOX. This may be related to increased drug uptake and effective intracellular drug release.

In vitro Cellular Uptake

The cellular uptake of DOX and CTPA@DOX was detected using CLSM. At the time point of 4 h, a strong red fluorescence (DOX fluorescence) intensity was observed in the CTPA@DOX group, and a higher fluorescence intensity

was observed at 24 h (Figure 5A and B). This phenomenon demonstrated that CTPA@DOX entered cells in a time-dependent manner. Although free DOX gradually entered the cells, its fluorescence intensity was notably weaker (Figure 5A and B). Moreover, the flow cytometry analysis also reveals the intracellular fluorescence intensity of DOX, which is effective comments on the uptake of nanodrugs by CAL-27 cells at 24 h, which is consistent with CLSM result. Quantitative assessment of cellular uptake in the CTPA@DOX group showed that the amount of DOX internalised into cells increased 6.7-fold over that of free DOX at 24 h (Figure 5C and D). This result was attributed to the fact that CTPA@DOX penetrated the cell membrane through endocytosis, whereas free DOX passively diffused into cells with poor efficacy.⁴⁴ It is well documented that CTS possesses abundant bio-reactive groups. These groups can play a critical role in material-cell recognition and adherence through non-covalent routines, which facilitate endocytosis of CTS-based nanocarriers.⁴⁵ Therefore, PAA-modified CTS nanogels with derivable hydroxyl, amino, and carboxyl groups can be used as matrices for the fabrication of theranostic nanoplateforms.

Evaluation of CT Imaging Ability

Therapeutic nanocarriers exhibit different therapeutic effects in different diseases, synergistically enter the tumour with chemotherapeutic drugs in vivo, and exhibit excellent CT imaging capabilities.^{46,47} The X-ray attenuation property of CTPA@DOX was first examined in vitro to evaluate the potential of CTPA@DOX for CT imaging. It was observed that the higher the AuNP concentration, the more prominent the brightness of CT imaging (Figure 6A). Quantitative analysis showed that CT values presented a positive linear correlation with increasing AuNP concentration (Figure 6B), which sets the foundation for diagnostic application in vivo.

CT scans were performed to examine the feasibility of using CTPA@DOX as an imaging agent in vivo. At 1 h post-injection of CTPA@DOX, bright tumour tissue could be clearly observed in the sagittal, transverse, and coronal dimensions, whereas no significant difference was observed in the surrounding normal tissues (Figure 6C). As the imaging contrast is dependent on the molar concentration of AuNPs, the high contrast presented here demonstrated a large amount of AuNPs in the tumour. These results infer that CTPA@DOX had favourable tumour accumulation and effective conjugation with AuNPs. Collectively, CTPA@DOX can be used as a self-tracking tool to evaluate drug delivery status.

In vivo Anti-Tumour Activity

The anti-tumour effect was assessed in OSCC-bearing nude mice after treatment with PBS, CTPA@DOX, and DOX. As shown in Figure 7A, tumours in mice treated with PBS and DOX grew continuously. In contrast, the tumour volume of the CTPA@DOX group decreased remarkably during the first 13 d, followed by a gradual increase after the complete release of DOX from CTPA. On day 21, tumours were collected from all treated mice. It was found CTPA@DOX treatment strongly inhibited tumour growth (Figure 7C and D). These results indicate a higher anti-tumour activity of CTPA@DOX than that of free DOX at the same concentration of DOX. In addition, no significant difference in body weight was observed among the three groups (Figure 7B), demonstrating that CTPA@DOX possessed preferable biocompatibility and negligible system toxicity.

Furthermore, tumour tissues were treated with H&E and TUNEL staining to verify the anti-tumour effect. H&E staining revealed extensive karyorrhexis, karyopyknosis, and karyolysis, which represents severe destruction of tumour cells, in the CTPA@DOX group (Figure 7E). TUNEL assays showed a high proportion of apoptotic cells in CTPA@DOX-treated tumours, which was in accordance with the findings of H&E staining (Figure 7F). Therefore, it can be inferred that CTPA@DOX possesses a strong inhibitory effect against tumours, which was likely because of good passive targeting, effective drug release, and enhanced cell internalisation.

The biosafety of CTPA@DOX was also assessed at the tissue level. At day 21 post-injection, the primary organs (liver, heart, lungs, kidneys, and spleen) were resected for H&E staining. As expected, no clear abnormalities were observed in any of the experimental groups, indicating that CTPA@DOX can be safely applied in vivo (Figure 8). Additionally, organ coefficients and biochemical parameters (that is, alanine transaminase (ALT), aspartate aminotransferase (AST), alkaline phosphatase (ALP), blood urea nitrogen (BUN), and creatinine (CRE)) were measured to confirm the biocompatibility of CTPA@DOX. As shown in Figure 9, the levels of the relevant indicators in the CTPA@DOX

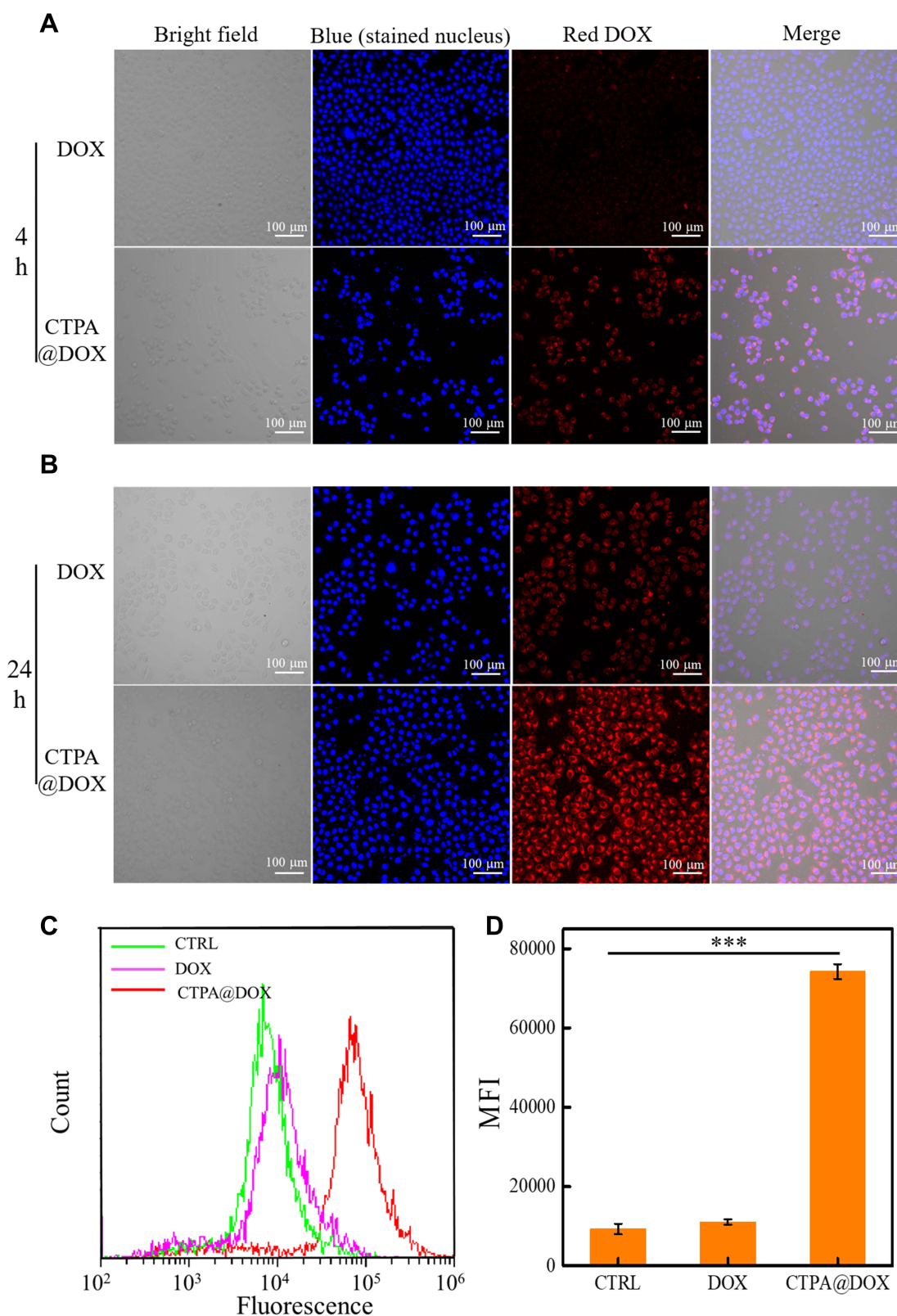


Figure 5 CLSM images of DOX- and CTPA@DOX-treated CAL27 cells at (A) 4 h and (B) 24 h; (C) the flow Cytometry Measurement of Fluorescence Levels of Intracellular DOX in CAL-27 Cells at 24 h; (D) Corresponding mean fluorescence intensity. ***Represents $P < 0.001$.

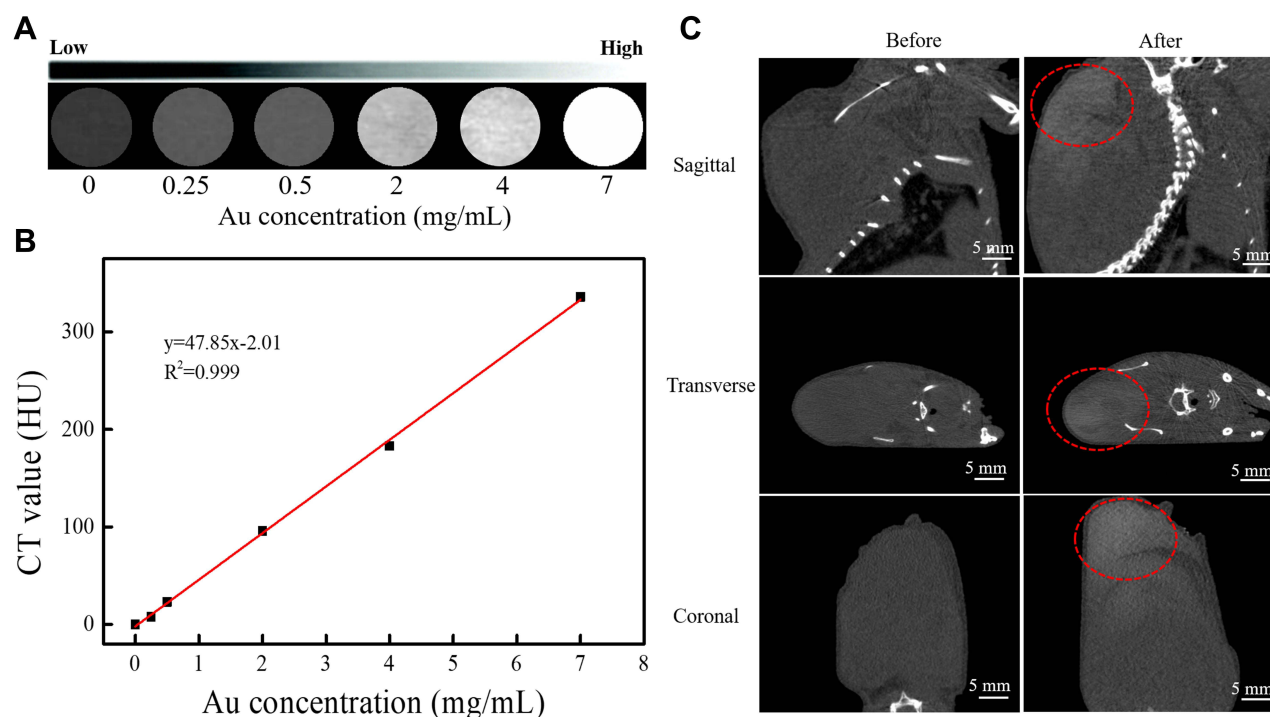


Figure 6 (A) CT images of CTPA@DOX suspended in agar; (B) CT value plotted against various concentrations of AuNPs; (C) CT scan imaging of mice with sagittal, transverse, and coronal dimensions before and after intravenous administration of CTPA@DOX. The white section in the red circle represents the contrast image of the nanomedicine in mice.

group were similar to those in the PBS group and were slightly lower than those in the DOX group. These findings suggest that CTPA@DOX had superior compatibility and attenuated the toxicity of DOX.

Several CTS NPs and their nanohybrids with inorganic drug systems have been developed for the delivery of cationic drugs (such as DOX). It has been demonstrated that the addition of inorganic particles can increase the functionality and drug-loading capacity of CTS NPs.⁴⁸ However, these platforms lack imaging and efficient drug degradation at tumour sites. In this study, a surface assembly strategy was employed to adapt the surface charge of the NPs for efficient drug delivery of the cationic drug DOX (87.1%), which was significantly higher than the reported loading efficiency of CTS nanocarriers for DOX (approximately 4%).⁴⁹ Importantly, nearly 80% of the loaded drug was released in a simulated *in vitro* microenvironment, which is higher than that of previous DOX-loaded inorganic nanosystems (for example, carbon nanotubes (CNTs) and mesoporous silica (MSN)).⁵⁰ These properties increase the ability of nanocarriers to deliver drugs in mice, showing great potential for targeted imaging of antitumour drugs.

Conclusion

In summary, hybrid nanogels based on natural macromolecules (such as CTS and sodium alginate) are more suitable than common inorganic carriers for delivering anticancer drugs because of their good biocompatibility and functionality. In this study, PAA-modified CTS nanogels were developed for the fabrication of a theranostic nanoplatform. AuNPs as CT contrast agents were efficiently conjugated to the exterior surface of the nanogels, whereas DOX as the chemotherapeutic agent was entrapped in the interior structure at a high encapsulation rate. The resultant theranostic nanoplatform, CTPA, exhibited the desired physical characteristics, including rational shape, size, charge, and colloidal stability, which enable a long circulation time. The size-shrink capability for deep tumour penetration, dual lysozyme and acid-responsive drug release for tumour-targeted therapy, and easy internalisation by tumour cells render CTPA@DOX an advanced drug delivery tool. As expected, CTPA exhibited good biocompatibility, and CTPA@DOX showed an enhanced inhibitory effect on tumour cells *in vitro*. Through a human OSCC-bearing mouse model, CTPA@DOX exhibited superior

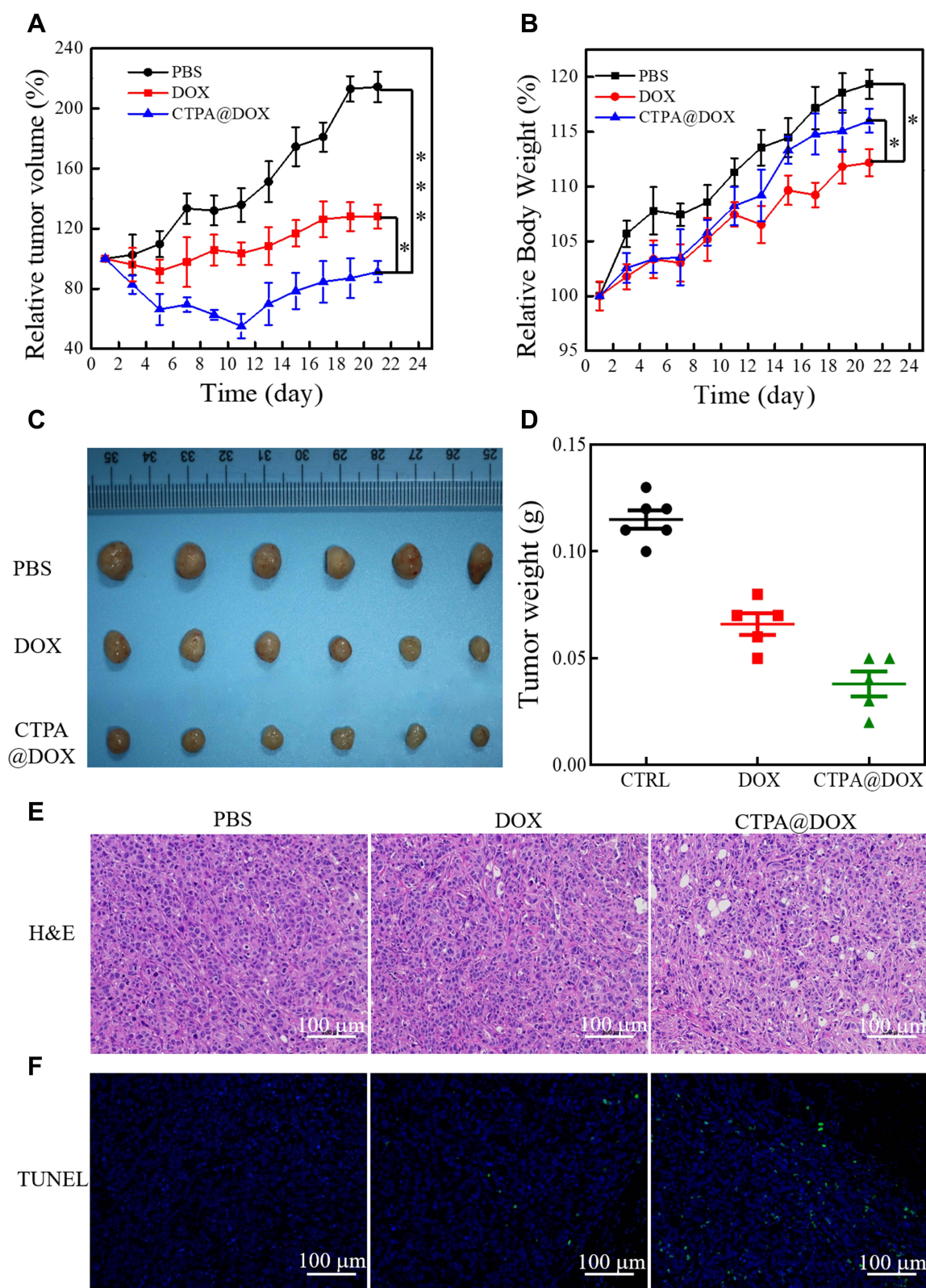


Figure 7 Evaluation of antitumor activity in vivo. **(A)** Alterations of tumour volume of mice treated with PBS, DOX, and CTPA@DOX for 21 d; **(B)** Alteration of body weight of mice treated with PBS, DOX, and CTPA@DOX for 21 d; **(C)** Digital images of excised tumours on the 21st day after treatment; **(D)** Tumour weight on the 21st day post-injection; **(E)** H&E staining of tumour sections; **(F)** TUNEL staining of tumour sections. The 6 samples are used for repeated analysis of differences between different tissue sections ($n=6$). *Represents $P < 0.05$ and ***represents $P < 0.001$.

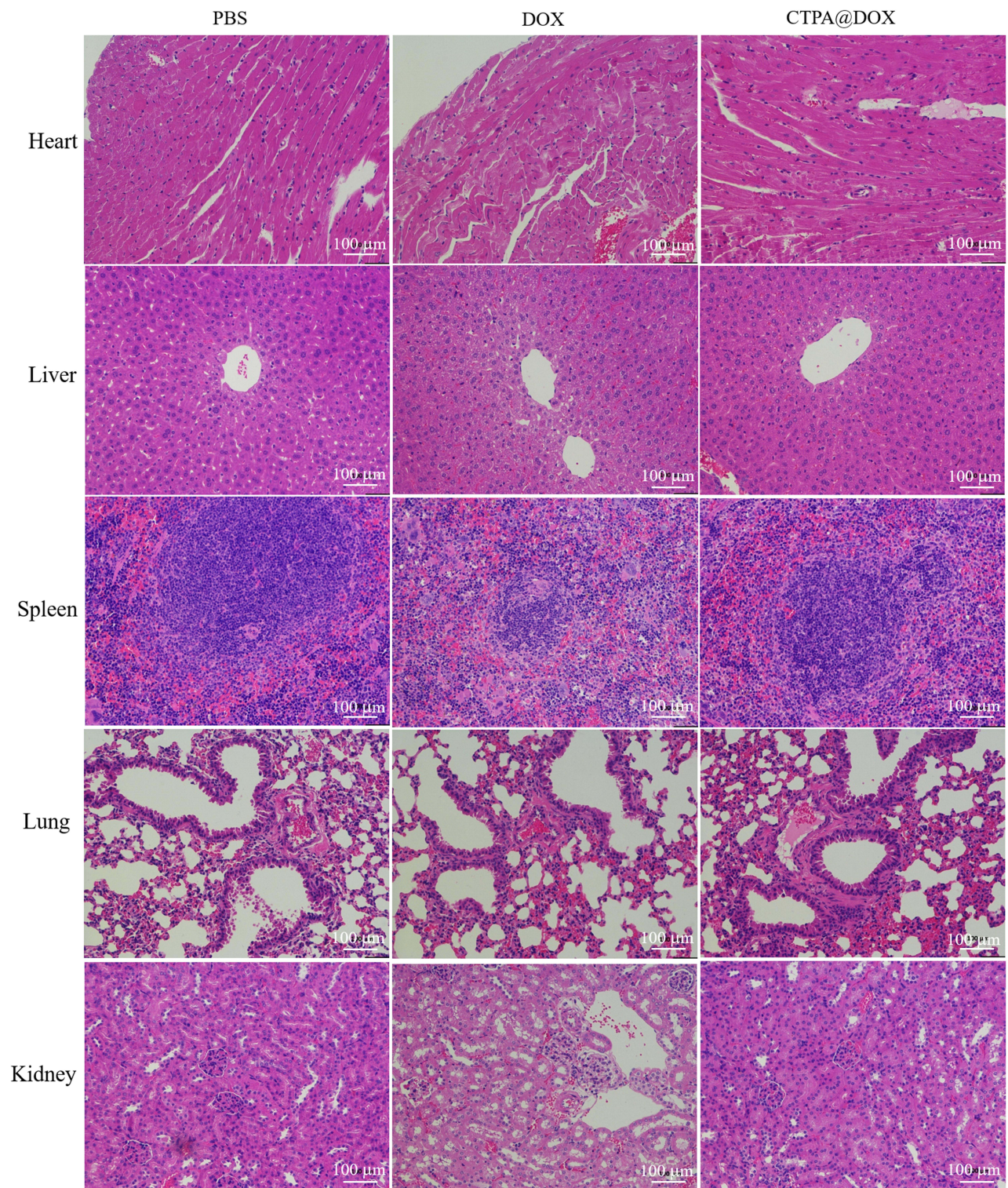


Figure 8 H&E staining images of the main organs (heart, liver, spleen, lungs, and kidneys) of mice treated with PBS, DOX, and CTPA@DOX. The 6 samples are used for repeated analysis of differences between different tissue sections (n=6).

biosafety and therapeutic efficiency compared to free DOX. Owing to the introduction of AuNPs, CTPA@DOX enabled monitoring of the drug delivery status at the treatment dosage. These benefits suggest that this hybrid theranostic nanogel holds great potential for future clinical applications.

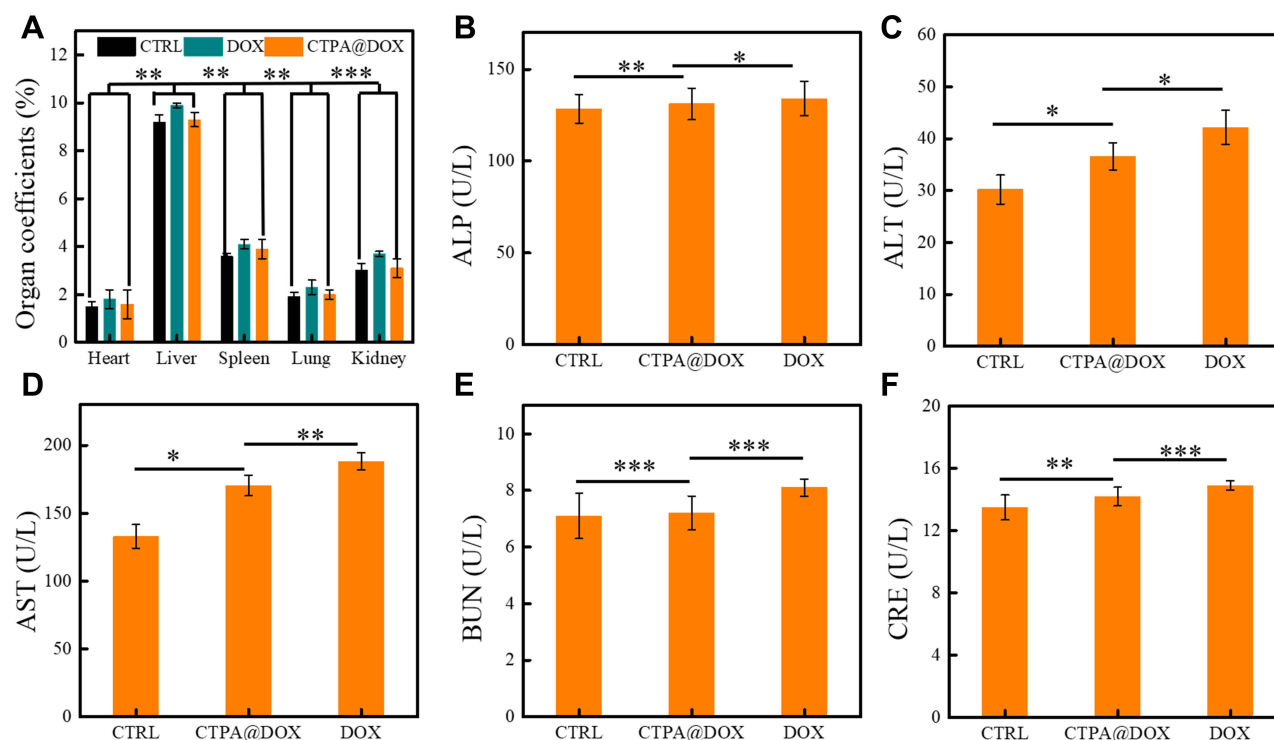


Figure 9 (A) The organ coefficients of heart, liver, spleen, lungs, and kidneys; Blood biochemistry parameters of the mice, including (B) ALP, (C) ALT, (D) AST, (E) BUN, and (F) CRE. *Represents $P < 0.05$, **represents $P < 0.01$, and ***represents $P < 0.001$.

Abbreviations

CCK-8, Cell Counting Kit 8; DMEM, Dulbecco's modified Eagle's medium; DOX, doxorubicin; FBS, foetal bovine serum; AuNPs, gold nanoparticles; CTS, chitosan; TPP, tripolyphosphate; PAA, polyacrylic acid; CTP, chitosan/sodium tripolyphosphate/polyacrylic acid; CTPA, chitosan/sodium tripolyphosphate/polyacrylic acid@gold nanoparticles; RES, reticuloendothelial system; CT, computed tomography; H&E, haematoxylin and eosin; PBS, phosphate-buffered saline; TEM, transmission electron microscopy; SEM, Scanning electron microscopy; TUNEL, terminal deoxynucleotidyl transferase-mediated dUTP-biotin nick-end labelling.

Acknowledgments

This work was supported by the National Natural Science Foundation of China (no. 82160194 and no. 81960492), the Natural Science Foundation of Jiangxi Province (20181ACB20022) and the Key Research and Development Program of Jiangxi Province (20212BBG73022).

Disclosure

The authors declare no conflicts of interest in this work.

References

- Mu J, Lin J, Huang P, Chen X. Development of endogenous enzyme-responsive nanomaterials for theranostics. *Chem Soc Rev*. 2018;47:5554–5573. doi:10.1039/C7CS00663B
- Panwar N, Soehartono AM, Chan KK, et al. Nanocarbons for biology and medicine: sensing, imaging, and drug delivery. *Chem Rev*. 2019;119(16):9559–9656. doi:10.1021/acs.chemrev.9b00099
- Laraib U, Sargazi S, Rahdar A, et al. Nanotechnology-based approaches for effective detection of tumor markers: a comprehensive state-of-the-art review. *Int J Biol Macromol*. 2021;195:356–383. doi:10.1016/j.ijbiomac.2021.12.052
- Gholami A, Mousavi SM, Hashemi SA, et al. Current trends in chemical modifications of magnetic nanoparticles for targeted drug delivery in cancer chemotherapy. *Drug Metab Rev*. 2020;52(1):205–224. doi:10.1080/03602532.2020.1726943

5. Yang H, He Y, Wang Y, et al. Theranostic nanoparticles with aggregation-induced emission and MRI contrast enhancement characteristics as a dual-modal imaging platform for image-guided tumor photodynamic therapy. *Int J Nanomed.* 2020;15:3023–3038. doi:10.2147/IJN.S244541
6. Lim E-K, Kim T, Paik S, Haam S, Huh Y-M, Lee K. Nanomaterials for theranostics: recent advances and future challenges. *Chem Rev.* 2015;115:327–394. doi:10.1021/cr300213b
7. Barani M, Rahdar A, Sargazi S, et al. Nanotechnology for inflammatory bowel disease management: detection, imaging and treatment. *Sens Bio Sens Res.* 2021;32:100417. doi:10.1016/j.sbsr.2021.100417
8. Salmani MM, Hashemian M, Yekta HJ, et al. Synergic effects of magnetic nanoparticles on hyperthermia-based therapy and controlled drug delivery for bone substitute application. *J Supercond Nov Magn.* 2020;33(9):2809–2820. doi:10.1007/s10948-020-05530-1
9. Zhu J, Yang J, Zhao L, et al. (131) I-Labeled multifunctional polyethylenimine/doxorubicin complexes with pH-controlled cellular uptake property for enhanced SPECT imaging and chemo/radiotherapy of tumors. *Int J Nanomed.* 2021;16:5167–5183. doi:10.2147/IJN.S312238
10. Cai Y, Chen X, Si J, Mou X, Dong X. All-in-One nanomedicine: multifunctional single-component nanoparticles for cancer theranostics. *Small.* 2021;17:2103072. doi:10.1002/sml.202103072
11. Kim H, Kwak G, Kim K, Yoon HY, Kwon IC. Theranostic designs of biomaterials for precision medicine in cancer therapy. *Biomaterials.* 2019;213:119207. doi:10.1016/j.biomaterials.2019.05.018
12. Su S, M. Kang P. Recent advances in nanocarrier-assisted therapeutics delivery systems. *Pharmaceutics.* 2020;12:837. doi:10.3390/pharmaceutics12090837
13. Zhao Z, Ukidve A, Krishnan V, Mitragotri S. Effect of physicochemical and surface properties on in vivo fate of drug nanocarriers. *Adv Drug Deliv Rev.* 2019;143:3–21. doi:10.1016/j.addr.2019.01.002
14. Lee S, Pham TC, Bae C, Choi Y, Kim YK, Yoon J. Nano theranostics platforms that utilize proteins. *Coordin Chem Rev.* 2020;412:213258. doi:10.1016/j.ccr.2020.213258
15. Wang H, Chen Q, Zhou S. Carbon-based hybrid nanogels: a synergistic nanoplatform for combined biosensing, bioimaging, and responsive drug delivery. *Chem Soc Rev.* 2018;47:4198–4232. doi:10.1039/C7CS00399D
16. Zhao Q, Zhang S, Wu F, et al. Rational design of nanogels for overcoming the biological barriers in various administration routes. *Angew Chem Int Edit.* 2021;60:14760–14778. doi:10.1002/anie.201911048
17. Hajebi S, Rabiee N, Bagherzadeh M, et al. Stimulus-responsive polymeric nanogels as smart drug delivery systems. *Acta Biomater.* 2019;92:1–18. doi:10.1016/j.actbio.2019.05.018
18. Molina M, Asadian-Birjand M, Balach J, Bergueiro J, Miceli E, Calderon M. Stimuli-responsive nanogel composites and their application in nanomedicine. *Chem Soc Rev.* 2015;44:6161–6186. doi:10.1039/c5cs00199d
19. Anselmo AC, Zhang M, Kumar S, et al. Elasticity of nanoparticles influences their blood circulation, phagocytosis, endocytosis, and targeting. *ACS Nano.* 2015;9:3169–3177. doi:10.1021/acsnano.5b00147
20. Desai P, Rimal R, Florea A, et al. Tuning the elasticity of nanogels improves their circulation time by evading immune cells. *Angew Chem Int Edit.* 2022;61:e202116653. doi:10.1002/anie.202116653
21. Myerson JW, McPherson O, DeFrates KG, et al. Cross-linker-modulated nanogel flexibility correlates with tunable targeting to a sterically impeded endothelial marker. *ACS Nano.* 2019;13:11409–11421. doi:10.1021/acsnano.9b04789
22. Nagel G, Sousa-Herves A, Wedepohl S, Calderón M. Matrix metalloproteinase-sensitive multistage nanogels promote drug transport in 3D tumor model. *Theranostics.* 2020;10:91–108. doi:10.7150/thno.34851
23. Swierczewska M, Han HS, Kim K, Park JH, Lee S. Polysaccharide-based nanoparticles for theranostic nanomedicine. *Adv Drug Deliv Rev.* 2016;99:70–84. doi:10.1016/j.addr.2015.11.015
24. Pérez-álvarez L, Ruiz-Rubio L, Artetxe B, Vivanco M, Gutiérrez-Zorrilla JM, Vilas-Vilela JL. Chitosan nanogels as nanocarriers of polyoxometalates for breast cancer therapies. *Carbohydr Polym.* 2019;213:159–167. doi:10.1016/j.carbpol.2019.02.091
25. Wang H, Qian J, Ding F. Recent advances in engineered chitosan-based nanogels for biomedical applications. *J Mater Chem B.* 2017;5:6986–7007. doi:10.1039/C7TB01624G
26. Li Y, Maciel D, Rodrigues J, Shi X, Tomás H. Biodegradable polymer nanogels for drug/Nucleic Acid delivery. *Chem Rev.* 2015;115:8564–8608. doi:10.1021/cr500131f
27. Avramović N, Mandić B, Savić-Radojević A, Simić T. Polymeric nanocarriers of drug delivery systems in cancer therapy. *Pharmaceutics.* 2020;12:298. doi:10.3390/pharmaceutics12040298
28. Han X, Xu K, Taratula O, Farsad K. Applications of nanoparticles in biomedical imaging. *Nanoscale.* 2019;11(3):799–819. doi:10.1039/C8NR07769J
29. Lusic H, Grinstaff MW. X-ray-computed tomography contrast agents. *Chem Rev.* 2013;113:1641–1666. doi:10.1021/cr200358s
30. Wu Y, Ali MRK, Chen K, Fang N, El-Sayed MA. Gold nanoparticles in biological optical imaging. *Nano Today.* 2019;24:120–140. doi:10.1016/j.nantod.2018.12.006
31. Lee B, Lee K, Panda S, et al. Nanoparticle delivery of CRISPR into the brain rescues a mouse model of fragile X syndrome from exaggerated repetitive behaviours. *Nat Biomed Eng.* 2018;2:497–507. doi:10.1038/s41551-018-0252-8
32. Luther DC, Huang R, Jeon T, et al. Delivery of drugs, proteins, and nucleic acids using inorganic nanoparticles. *Adv Drug Deliv Rev.* 2020;156:188–213. doi:10.1016/j.addr.2020.06.020
33. Li J, Chen L, Xu X, et al. Targeted combination of antioxidative and anti-inflammatory therapy of rheumatoid arthritis using multifunctional dendrimer-entrapped Gold nanoparticles as a platform. *Small.* 2020;16:2005661. doi:10.1002/sml.202005661
34. Sun W, Zhang J, Zhang C, et al. A unique nanogel-based platform for enhanced dual mode tumor MR/CT imaging. *J Mater Chem B.* 2018;6:4835–4842. doi:10.1039/C8TB01044G
35. Veeren A, Ogunyankin MO, Shin JE, Zasadzinski JA. Liposome-tethered gold nanoparticles triggered by pulsed NIR light for rapid liposome contents release and endosome escape. *Pharmaceutics.* 2022;14:701. doi:10.3390/pharmaceutics14040701
36. Hu D, Deng Y, Jia F, Jin Q, Ji J. Surface charge switchable supramolecular nanocarriers for nitric oxide synergistic photodynamic eradication of biofilms. *ACS Nano.* 2020;14:347–359. doi:10.1021/acsnano.9b05493
37. Niu Y, Zhu J, Li Y, et al. Size shrinkable drug delivery nanosystems and priming the tumor microenvironment for deep intratumoral penetration of nanoparticles. *J Control Release.* 2018;277:35–47. doi:10.1016/j.jconrel.2018.03.012
38. Serra C, Vizoso F, Alonso L, et al. Expression and prognostic significance of lysozyme in male breast cancer. *Breast Cancer Res.* 2002;4:R16. doi:10.1186/bcr537

39. Li H-J, Du J-Z, Du X-J, et al. Stimuli-responsive clustered nanoparticles for improved tumor penetration and therapeutic efficacy. *P Natl Acad Sci USA*. 2016;113:4164–4169. doi:10.1073/pnas.1522080113
40. Zhou D, Liu S, Hu Y, et al. Tumor-mediated shape-transformable nanogels with pH/redox/enzymatic-sensitivity for anticancer therapy. *J Mater Chem B*. 2020;8:3801–3813. doi:10.1039/D0TB00143K
41. Kang H, Gravier J, Bao K, et al. Renal clearable organic nanocarriers for bioimaging and drug delivery. *Adv Mater*. 2016;28:8162–8168. doi:10.1002/adma.201601101
42. Karimi M, Ghasemi A, Sahandi Zangabad P, et al. Smart micro/nanoparticles in stimulus-responsive drug/gene delivery systems. *Chem Soc Rev*. 2016;45:1457–1501. doi:10.1039/C5CS00798D
43. Ahmed TA, Aljaeid BM. Preparation, characterization, and potential application of chitosan, chitosan derivatives, and chitosan metal nanoparticles in pharmaceutical drug delivery. *Drug Des Devel Ther*. 2016;10:483–507. doi:10.2147/DDDT.S99651
44. Wang S, Wu X, Tan M, et al. Fighting fire with fire: poisonous Chinese herbal medicine for cancer therapy. *J Ethnopharmacol*. 2012;140:33–45. doi:10.1016/j.jep.2011.12.041
45. Akbari-Alavijeh S, Shaddel R, Jafari SM. Encapsulation of food bioactives and nutraceuticals by various chitosan-based nanocarriers. *Food Hydrocolloid*. 2020;105:105774. doi:10.1016/j.foodhyd.2020.105774
46. Faghfoori MH, Nosrati H, Rezaeejam H, et al. Anticancer effect of X-Ray triggered methotrexate conjugated albumin coated bismuth sulfide nanoparticles on SW480 colon cancer cell line. *Int J Pharmaceut*. 2020;582:119320. doi:10.1016/j.ijpharm.2020.119320
47. Nosrati H, Attari E, Abhari F, et al. Complete ablation of tumors using synchronous chemoradiation with bimetallic theranostic nanoparticles. *Bioact Mater*. 2022;7:74–84. doi:10.1016/j.bioactmat.2021.05.015
48. Bernkop-Schnürch A, Dünnhaupt S. Chitosan-based drug delivery systems. *Eur J Pharm Biopharm*. 2012;81(3):463–469. doi:10.1016/j.ejpb.2012.04.007
49. Kango S, Kalia S, Celli A, et al. Surface modification of inorganic nanoparticles for development of organic–inorganic nanocomposites—A review. *Prog Polym Sci*. 2013;38(8):1232–1261. doi:10.1016/j.progpolymsci.2013.02.003
50. Chen Y, Chen H, Shi J. Inorganic nanoparticle-based drug codelivery nanosystems to overcome the multidrug resistance of cancer cells. *Mol Pharmaceut*. 2014;11(8):2495–2510. doi:10.1021/mp400596v

International Journal of Nanomedicine

Dovepress

Publish your work in this journal

The International Journal of Nanomedicine is an international, peer-reviewed journal focusing on the application of nanotechnology in diagnostics, therapeutics, and drug delivery systems throughout the biomedical field. This journal is indexed on PubMed Central, MedLine, CAS, SciSearch®, Current Contents®/Clinical Medicine, Journal Citation Reports/Science Edition, EMBase, Scopus and the Elsevier Bibliographic databases. The manuscript management system is completely online and includes a very quick and fair peer-review system, which is all easy to use. Visit <http://www.dovepress.com/testimonials.php> to read real quotes from published authors.

Submit your manuscript here: <https://www.dovepress.com/international-journal-of-nanomedicine-journal>